J. Fluid Mech. (1994), *vol.* 274, *pp.* 115–138

Finite-size effects in forced two-dimensional turbulence

By LESLIE M. SMITH† AND VICTOR YAKHOT

Program in Applied and Computational Mathematics, Princeton University, Princeton, NJ 08544, USA

(Received 27 August 1993 and in revised form 28 February 1994)

A new mechanism for the creation of structures in two-dimensional turbulence is investigated. The forced Navier–Stokes equations are solved numerically in a periodic square in the limit of zero viscosity. The force is a white-in-time random noise acting in a narrow band of high wavenumbers. The inverse-cascade process and the presence of the boundary lead ultimately to a pile-up of energy in the lowest wavenumber (Bose condensation). In the asymptotic limit where the enstrophy cascade range is negligible, Bose condensation is solely responsible for the generation of coherent vortices and intermittency in the system. We present the evolution of the velocity and vorticity fields through the later stages of the condensate state, and explore the possible implications for atmospheric turbulence constrained by the periodic domain about the earth.

1. Introduction

One of the major challenges of the turbulence problem is to understand the origin and significance of long-living, coherent structures that usually exist within a background of random fluctuations. The presence of coherent structures causes the normalized moments of velocity differences to be displacement-dependent rather than constant as for a purely Gaussian field. There has been an effort to parameterize the displacement dependence of the normalized moments, but little is known about the mechanisms governing the formation and behaviour of the structures responsible for this effect. In particular, it is important to separate the role of external parameters from the internal dynamics of the nonlinear term. Among the external parameters that may characterize a turbulent flow are the power of the energy source ϵ and the lengthscales L and l_0 corresponding respectively to the size of the system and the energy-input scale.

In a step towards understanding the roles of ϵ, L and l_0 for structure generation in two-dimensional turbulence, we numerically studied Bose condensation in isotropic two-dimensional turbulence driven by a white-in-time random force localized about the small scale l_0 (Smith & Yakhot 1993). Bose condensation in two-dimensional turbulence was predicted by Kraichnan (1967) and confirmed numerically by Hossain, Matthaeus & Montgomery (1983), and refers to energy accumulation in the lowest wavenumber defining the boundary of the system. In our recent numerical simulations, we studied the inverse cascade of energy in two-dimensional turbulence under conditions designed to simulate very high Reynolds number and negligible influence of the enstrophy cascade range. We observed that during the cascade of energy to large scales but before formation of the condensate at the largest scale, the flow is structureless and the normalized even-order moments of velocity differences are

† Present address: Department of Mechanical Engineering, Yale University, New Haven, CT 06520, USA

Gaussian. The appearance of isolated vortices, reflected by the displacement dependence of the normalized moments, occurs only after energy accumulates in the largest scale because of the finite extent of the domain. Thus, in this case, intermittency is a finite-size effect. Here we wish to further explore the consequences of finite boundaries and the accompanying phenomenon of Bose condensation in two-dimensional turbulence. To fully isolate the dynamics of the large scales, we continue to restrict the parameter values of our numerical simulations such that the forward cascade of enstrophy to small scales is unimportant.

The creation of coherent structures is important in atmospheric science and has attracted the attention of various investigators (Overman & Zabusky 1982; Flierl, Stern & Whitehead 1983; Benzi, Paternello & Santangelo 1988; Melander, Zabusky & McWilliams 1987, 1988; McWilliams 1989). It has been shown that strong vortices are formed as a result of the merger of smaller and weaker ones originating from the nonlinear dynamics at the small scales. In this paper, we consider a new mechanism of vortex generation resulting from the creation of box-size motions. Owing to the inverse energy cascade in two-dimensional turbulence, the formation of these large-scale eddies is inevitable, and thus the mechanism considered in this paper might be of general importance.

In §2, we give the basic equations to be solved and show how simple arguments based on dimensional analysis and naive power counting lead to the prediction for energy spectrum $E(k) \propto k^{-5/3}$ in a quasi-steady state for wavenumbers smaller than the forcing wavenumber and larger than the inverse-integral scale. The numerical simulations presented in the following sections give support to this simple picture of two-dimensional turbulence in the inverse-cascade range for the case in which there is negligible enstrophy flux in this range ($k < k_0 = 2\pi/l_0$). In §3, we review the results of the forced simulation in $1 \leqslant k$ given by Smith & Yakhot (1993) for comparison with new simulations having altered boundary conditions. Section 4 describes the formation of a lattice of vortices when the flow is restricted to wavenumbers k in the range $k_T \leqslant k$, where the value of the truncation wavenumber is taken to be $k_T = 11$. Section 5 presents the flow damped by an Ekman friction at low wavenumbers and compares the energy spectrum to observed atmospheric spectra (Lilly & Peterson 1983; Nastrom, Gage & Jasperson 1984). Section 6 describes the mechanism for vortex generation due to finite-size effects, which is different from both vortex generation due to the direct cascade of enstrophy and vortex merger in decaying turbulence. In §7 we discuss the implications of this work and future research directions.

2. The equations

We consider forced two-dimensional incompressible flow damped at small scales by viscosity and at large scales by linear friction,

$$\frac{\partial \omega}{\partial t} - \frac{\partial \psi}{\partial x}\frac{\partial \omega}{\partial y} + \frac{\partial \psi}{\partial y}\frac{\partial \omega}{\partial x} = \nabla \times \boldsymbol{f} + \nu(-1)^{p+1}(\nabla^2)^p \omega - \alpha\omega, \tag{1}$$

where ψ is the streamfunction, $\omega = -\nabla^2\psi$ is the vorticity, $\boldsymbol{f}$ is the force, ν is the viscosity and α is the damping frequency. The velocity $\boldsymbol{v}$ is given in terms of the streamfunction by $u = \partial\psi/\partial y$ and $v = -\partial\psi/\partial x$. Equation (1) reduces to the Navier–Stokes equations for $p = 1$ and $\alpha = 0$. For appropriate choices of the viscosity ν, the domain in which the viscous term is significant can be restricted to increasingly higher wavenumbers as p increases. Thus for fixed resolution, the effective Reynolds number can be made higher with $p \geqslant 2$. In our simulations we use a hyperviscosity with $p = 8$, which allows

for the existence of a sizeable inertial range where the action of viscosity is negligible. The force f is taken to be Gaussian and white-noise in time, defined by its correlation function

$$\langle f_i(\boldsymbol{k}, t) f_j(\boldsymbol{k}', t') \rangle \propto D(k)\, \delta(\boldsymbol{k}+\boldsymbol{k}')\, \delta(t-t'). \tag{2}$$

As we are interested in the inverse cascade of energy from high to low wavenumbers, we take $D(k)$ to be localized about the high wavenumber k_0. For example, a convenient choice for theoretical analysis is

$$D(k) = 2\epsilon \frac{\delta(k^2 - k_0^2)}{k^{d-2}}, \tag{3}$$

where d is the dimension of space and ϵ is the kinetic energy production rate which in a statistically steady state is balanced by the dissipation.

2.1. *Energy continuity*

The continuity equation following from (1)–(3) is

$$\frac{\partial E(k)}{\partial t} + T(k) = kD(k) - 2\nu k^{2p} E(k) - 2\alpha E(k), \tag{4a}$$

where $E(k)$ is the energy spectrum. The energy transfer function $T(k)$ is the net rate of transfer into wavenumber k from interactions with wavenumbers p and q, and is given by

$$T(k) = \frac{1}{2} \int_0^\infty \int_0^\infty \mathrm{d}p\, \mathrm{d}q\, T(k, p, q), \tag{4b}$$

where the expression for $T(k, p, q)$ can be found in the standard literature (Kraichnan 1967) and $T(k, p, q) = T(k, q, p)$. Integrating (4) leads to

$$-J(k) = \int_k^\infty zD(z)\, \mathrm{d}z - 2\nu \int_k^\infty z^{2p} E(z)\, \mathrm{d}z - 2\alpha \int_k^\infty E(z)\, \mathrm{d}z - \frac{\partial K(k)}{\partial t}, \tag{5a}$$

where

$$J(k) = \int_0^k T(z)\, \mathrm{d}z = -\int_k^\infty T(z)\, \mathrm{d}z \tag{5b}$$

is the flux of energy through wavenumber k and

$$K(k) = \int_k^\infty E(z)\, \mathrm{d}z. \tag{5c}$$

To reduce the number of external parameters we set $\nu = \alpha = 0$ in relation (5a). In this case a statistically steady state is impossible since $J(0) = 0$ and thus the total energy $K = K(0) = \epsilon t$. However, consider the situation where the energy spectrum at $k > k_0$ decreases rapidly with k. In this case $K(k)$ for $k > k_0$ is small and the energy flux towards small scales can be neglected: $J(k) \approx 0$ at $k > k_0$. Then a statistically steady state is still possible in the sub-domain $k_i(t) \ll k < k_0$, leading to $J(k) = -\epsilon$ for $k_i(t) \ll k < k_0$ and $J(k) = 0$ for $k \ll k_i$. This is a situation considered in great detail in this paper. With ϵ, k_0 and $k_i(t)$ as the relevant parameters, the most general form of self-similar solution is

$$E(k) = C_K \epsilon^{2/3} k^{-5/3} \left(\frac{k}{k_i(t)}\right)^{-x+5/3} \left(\frac{k}{k_0}\right)^{-\gamma} \phi\left(\frac{k}{k_i(t)}\right), \tag{6}$$

where the dimensionless scaling function $\phi(z) \to 1$ when $z \gg 1$ and $\phi(z) \to 0$ when $z \ll 1$. Integrating (6) over $0 \leqslant k \leqslant \infty$ leads to

$$K = \epsilon t = C_1 \epsilon^{2/3} k_0^{\gamma} k_i^{-\gamma-2/3}(t), \tag{7a}$$

$$C_1 = C_K \int_0^{\infty} q^{-x-\gamma} \phi(q)\, \mathrm{d}q. \tag{7b}$$

Solving for $k_i(t)$ gives

$$k_i(t) = \left(\frac{C_1 k_0^{\gamma}}{\epsilon^{1/3} t}\right)^{1/(\gamma+2/3)}, \tag{8}$$

which is similar to a relation derived by Kraichnan (1967).

Although a steady state cannot exist for $0 \leqslant k \leqslant \infty$, (5) and (6) allow a state where only the modes $k \gg k_i(t)$ are statistically steady. In this quasi-steady state, the only possible exponent is $x = \frac{5}{3}$ and the spectrum is given by

$$E(k) = C_K \epsilon^{2/3} k^{-5/3} \left(\frac{k}{k_0}\right)^{-\gamma}, \quad k_i(t) \ll k < k_0. \tag{9}$$

Thus if a quasi-steady state exists for $k \gg k_i(t)$, then there is no influence of the infrared cutoff $k_i(t)$ on these modes, and one may conclude that infrared divergences appearing in renormalized perturbation theories must sum to zero. In this formulation of the problem, the complexity of two-dimensional turbulence is reduced to the analysis of the ultraviolet divergences in the vicinity of $k = k_0$. In a truly statistically steady state with the inverse energy cascade stabilized at the large scales by external fields, one cannot so easily rule out the possibility of infrared divergences and corresponding corrections to the Kolmogorov spectrum.

As will be shown in §3, our simulations with $\alpha = 0$ and $\nu \to 0$ support the existence of the quasi-steady state and the prediction $E(k) \propto k^{-5/3}$ for the modes in the range $k_i(t) \ll k < k_0$. Furthermore, we will show that the transfer of energy into k is due to interactions with wavenumbers p and q where $k < p, q \leqslant 4k$. This local nature of the energy transfer occurs because there is a cancellation between the flux from non-local interactions with $p, q > 4k$ and a forward flux of energy which exists in the finite system. This cancellation eliminates the infrared divergences from the problem. We would like to emphasize that these results cannot be generalized to the steady-state situation with low-wavenumber dissipation in which there is a non-negligible flux of enstrophy through wavenumbers smaller than the forcing wavenumber.

Non-zero values of α and ν allow a statistically steady state in the full domain $0 \leqslant k \leqslant \infty$. The linear damping $\alpha\omega$ can be considered as a model of the earth's Ekman boundary layer on the vertically averaged equations of motion (Pedlosky 1979). In the equations for the velocity v_i, one expects a balance at large scales and long times between αv_i and the nonlinear term $v_j\, \partial v_i / \partial x_j$. Assuming that $\Delta v \equiv v_i(x + r\hat{\imath}) - v_i(x)$ scales as $\Delta v \propto r^q$, this balance leads to $q = 1$ and the energy spectrum

$$E(k) = O(k^{-2q-1}) = O(k^{-3}), \quad k = O(1/L). \tag{10}$$

The balance leading to (10) between Ekman friction and the nonlinear term does not correspond to a state of constant flux.

In all of the simulations discussed herein, we solve (1) with $p = 8$ in a periodic square using a pseudo-spectral parallel code (Jackson, She & Orszag 1991) at resolutions of 512^2 or 2048^2 Fourier modes. The force is taken to be (2) with $D(k) = A^2 k^{-6}/\Delta t$ in $k_0^l \leqslant k \leqslant k_0^h$, where k_0^l and k_0^h are the low- and high-wavenumber cutoffs of the force,

respectively, Δt is the time step and A is a fixed amplitude. We consider the case $\alpha = 0$ in §§3 and 4 and the case $\alpha \neq 0$ in §5.

3. The inverse-cascade of energy in a bounded domain

In §§3 and 4, we would like to emphasize the detailed dynamics of both the velocity and vorticity fields before and after condensation owing to finite-size effects. Section 3 deals with the simplest case of a finite box with $\boldsymbol{v}(\boldsymbol{k})$ non-zero for $1 \leqslant k$. Section 4 considers a more complicated situation in which energy is prevented from populating modes $\boldsymbol{v}(\boldsymbol{k})$ with $k \leqslant 10$. Although some of the velocity statistics of the former case were given previously (Smith & Yakhot 1993), we review them here for continuity.

3.1. *The energy spectrum*

To study the dynamics of the inverse-cascade range during the time when the inverse-integral scale $k_i(t)$ is smaller than the truncation wavenumber $k_T = 1$, we conducted a simulation with resolution of 2048^2 Fourier modes. This very high resolution allows for determination of scaling laws with more accuracy than has been previously achieved. Other investigators (e.g. Frisch & Sulem 1984; Maltrud & Vallis 1991) have simulated the inverse energy cascade range and concluded that the exponent of the energy spectrum was close to the Kolmogorov value $x = \frac{5}{3}$, but no error bar was calculated. In our 2048^2 simulation, we find two decades where the scaling exponent is $x \approx \frac{5}{3}$, with error bar ± 0.05 (figures 1 and 2). Also in contrast to earlier works, the statistics of higher-order moments of velocity are addressed.

Figure 1 shows the time evolution of the energy spectrum, starting from initial condition $\boldsymbol{v}(\boldsymbol{k}) = 0$ for all k. The low and high wavenumbers of the force were $k_0^l = 500$ and $k_0^h = 525$, the force amplitude was $A = 0.156$ and the value of the hyperviscosity was $\nu = 6.1 \times 10^{-47}$. In the early time development, before the energy in modes $k < k_0^l$ reaches approximately the energy level of the forced modes, the spectrum has the shape $E(k) = a(t)k^0$ for $k < k_0^l$, where $a(t)$ increases as t increases. For these early times, the nonlinear term is weak in comparison with the force. At intermediate times, the Kolmogorov spectrum $E(k) \propto k^{-5/3}$ is established in the interval $k_i(t) < k < k_0^l$, and the inverse-integral scale $k_i(t)$ decreases in time according to (8). Figure 2 shows the compensated spectrum $k^{5/3}E(k)$ at the last time of figure 1, representative of these intermediate times. The energy flux $J(k)$ is a negative constant in the range $k_i(t) < k < k_0^l$ where the flow is statistically steady, and the enstrophy flux is negligible for $k < k_0^l$.

For later times when $k_i(t) \to 1$, the time development of the large scales became prohibitively slow in the 2048^2 simulation, and therefore it was necessary to repeat the experiment with the lower resolution of 512^2 Fourier modes. The 512^2 simulation was forced in the interval $k_0^l = 100 \leqslant k \leqslant k_0^h = 105$ and the superviscosity was $\nu = 4.0 \times 10^{-36}$. Figure 3 displays the compensated spectra $k^{5/3}E(k)$ for two times t_1 ($\times$) and t_2 ($\bigcirc$) after $k_i(t) = 1$, and clearly indicates the formation of the Bose condensate. The energy spectrum is given by

$$E(k,t) \approx b(t)\,\delta(k-1) + C_K\,\epsilon^{2/3}k^{-x} \tag{11}$$

in the range $1 \leqslant k < k_0^l$ with $x = \frac{5}{3} \pm 0.05$ and $C_K \approx 7.0$.

3.2. *The normalized even-order moments of velocity differences*

A striking feature of the pre-condensate flow is demonstrated in the insert of figure 2, showing for the 2048^2 run the second-order moment $S_2 = \langle (\Delta u)^2 \rangle$ and the normalized even-order moments $F_{2n} \equiv \langle (\Delta u)^{2n} \rangle / \langle (\Delta u)^2 \rangle^n$, $n = 2-4$. The value of the displacement

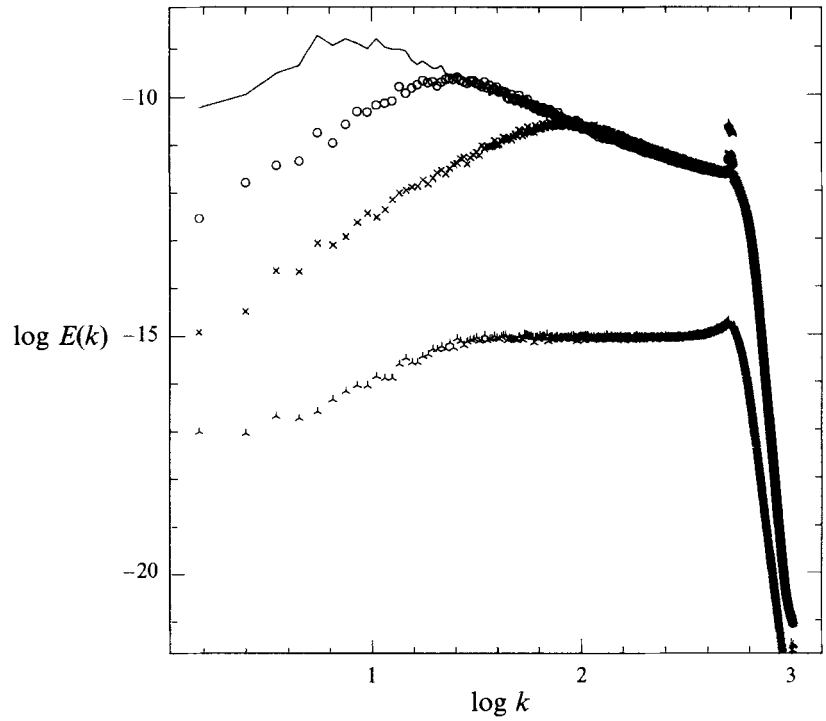

FIGURE 1. Time evolution (increasing upward) of the energy spectrum for the 2048^2 run.

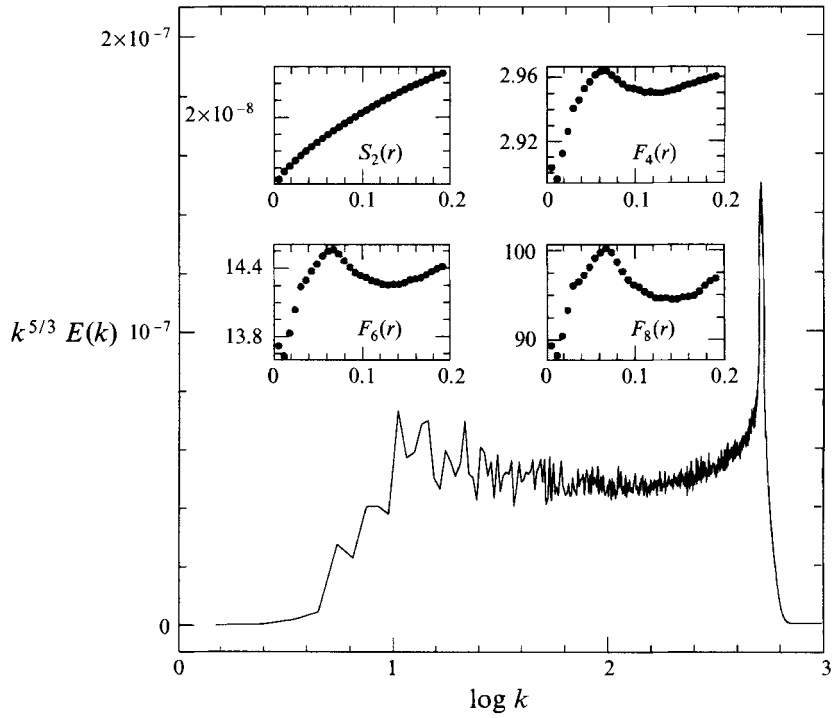

FIGURE 2. Compensated spectrum for the last time (solid curve) in figure 1. Insert: the second-order moment of velocity S_2 and the normalized moments F_{2n}, $n = 2-4$.

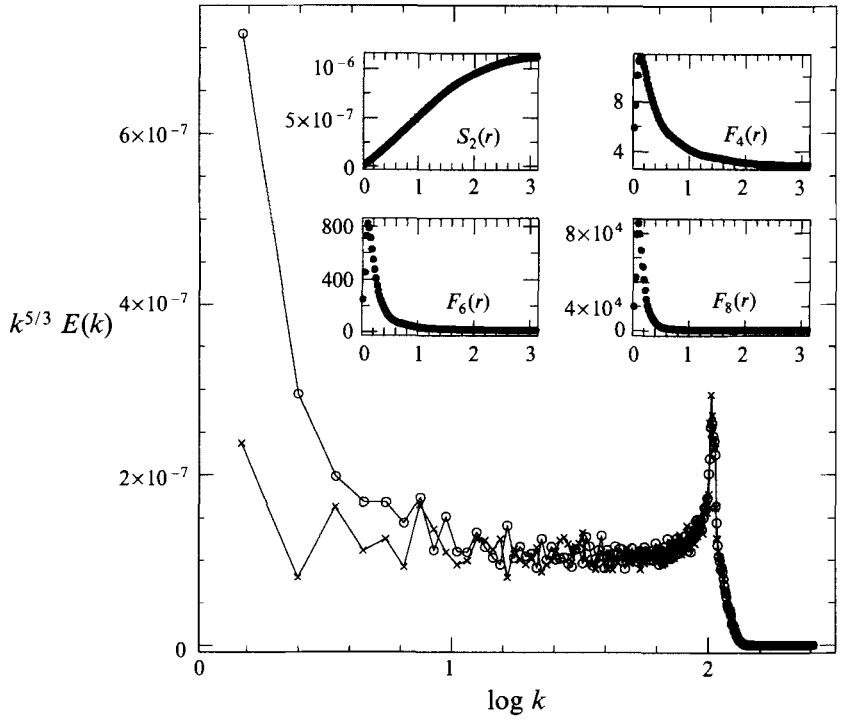

FIGURE 3. Compensated spectra ×, at an early time t_1 and ○, at a later time t_2 after condensation in the 512^2 run. Insert: S_2 and F_{2n}, $n = 2-4$ at t_2.

r corresponding to the input of energy is $r = 0.01$. One sees that the normalized even-order moments have a near-Gaussian distribution. Thus there is no intermittency in the high-Reynolds number flow before formation of the condensate.

The existence of the Kolmogorov spectrum $E(k) \propto k^{-5/3}$ indicates strong nonlinearity, but nevertheless the even-order moments of velocity differences do not deviate from the Gaussian values. We do not have a theoretical explanation of this fact, though some dynamical considerations are as follows. Let us assume that coherence is established as a result of interactions between the small-scale eddies of size r and velocity fluctuations of the integral scale $O(k_i^{-1}(t))$. The characteristic time of the process is of the order of the eddy-turnover time $\tau_i \propto k_i^{-2/3-\gamma}$ of the largest scales. However, according to (8), this is precisely the timescale of significant variation of $k_i(t)$. Even larger eddies, created as a result of the inverse cascade, tend to reduce the efficiency of coherence generation.

The insert of figure 3 shows S_2 and F_{2n}, $n = 2-4$ for time t_2 of the 512^2 run, where the energy-input scale is $r = 0.06$. One sees that the values of the normalized even-order moments remain the Gaussian values for $r > 1$. However, for small values of the displacement $r < 0.6$, the moments strongly deviate from the Gaussian values, indicating intermittency at small scales. Figure 4 shows S_2 and F_{2n} for the 512^2 run at the same two times t_1 and t_2 of figure 3, after formation of the condensate. Here the range of r has been reduced to emphasize the region of intermittency. Departure from the Gaussian values increases in time from t_1 to t_2 as the energy in wavenumber $k = 1$ increases. One sees that, in this system, small-scale intermittency is triggered by large-scale phenomena. Only after organized motions are established at the system size as a result of condensation, can small-scale structures with characteristic scale $O(k_0^{-1})$ be

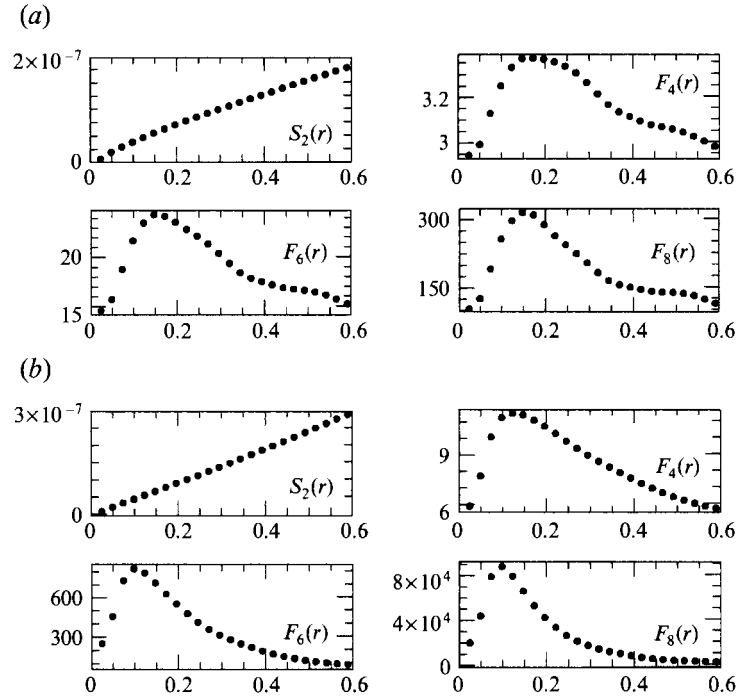

FIGURE 4. S_2 and F_{2n}, $n = 2-4$ for the 512^2 run at the two times of figure 3 (*a*) t_1; (*b*) t_2. The range of r has been reduced to emphasize the region of intermittency.

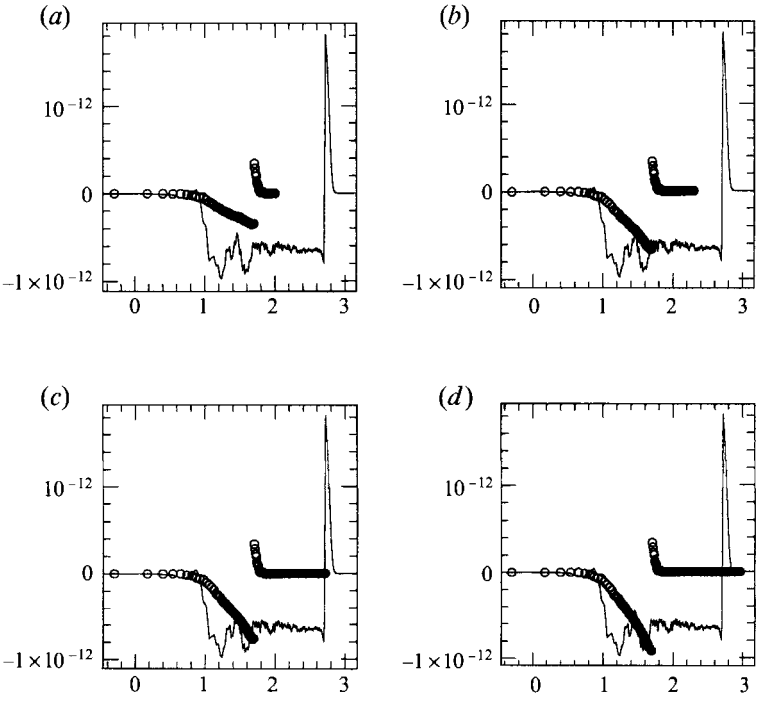

FIGURE 5. $J(k)$ (solid curve) and $J(k, k_1, k_f)$ (circles) for the 2048^2 run at the last time (solid curve) in figure 1 and $k_1 = 50$. (*a*) $k_f = 2k_1 = 100$; (*b*) $k_f = 4k_1 = 200$; (*c*) $k_f = 525$; (*d*) $k_f = 925$.

formed. The physical mechanism leading to the formation of these small-scale structures will be discussed in §6.

3.3. *The energy flux $J(k)$*

To determine which triads of wavenumbers contribute to the flux of energy $J(k_1)$ at wavenumber k_1 in the inverse-cascade range, we divided $J(k_1)$ following Kraichnan (1967)

$$J(k_1) = -\frac{1}{2}\int_0^{k_1} dk' \int_{k_1}^{\infty} dp \int_{k_1}^{\infty} dq\, T(k',p,q) + \frac{1}{2}\int_{k_1}^{\infty} dk' \int_0^{k_1} dp \int_0^{k_1} dq\, T(k',p,q), \quad (12)$$

where (12) is an exact representation of $J(k_1)$. The first integral is the total rate of energy loss to $k' < k_1$ from triad interactions with $p, q > k_1$ and the second integral is the total rate of energy input into the range $k' > k_1$ owing to triad interactions with $p, q < k_1$. We can classify the flux at k_1 as predominantly local or non-local by introducing the filter wavenumber k_f such that the filtered flux $J(k_1, k_f)$ is given by

$$J(k_1,k_f) = -\frac{1}{2}\int_0^{k_1} dk' \int_{k_1}^{k_f} dp \int_{k_1}^{k_f} dq\, T(k',p,q) + \frac{1}{2}\int_{k_1}^{k_f} dk' \int_0^{k_1} dp \int_0^{k_1} dq\, T(k',p,q). \quad (13)$$

The flux is local if a large percentage of the total is represented when k_f is nk_1 for n small, and conversely the flux is non-local if only a small percentage of the total is captured when k_f is nk_1. The notions of small and large will be made more precise below. As a visual aid, we plot the total flux $J(k)$ for all k together with

$$J(k,k_1,k_f) = \overbrace{-\frac{1}{2}\int_0^{k} dk' \int_{k_1}^{k_f} dp \int_{k_1}^{k_f} dq\, T(k',p,q)}^{J_1} + \overbrace{\frac{1}{2}\int_{k}^{k_f} dk' \int_0^{k_1} dp \int_0^{k_1} dq\, T(k',p,q)}^{J_2}, \quad (14)$$

where $0 \leqslant k < k_1$ in J_1 and $k_1 \leqslant k \leqslant k_f$ in J_2.

Figure 5 shows the total $J(k)$ (solid line) together with $J(k,k_1,k_f)$ (circles) for the 2048^2 run at the last time of figure 1 when the $k^{-5/3}$ spectrum extends over the range $k_i(t) \approx 10 < k < k_0^l = 100$. We took $k_1 = 50$ as a representative inertial-range wavenumber, and chose the filters $k_f = 100$, 200, 525 and 925. In each plot, the negative contribution to $J(k,k_1,k_f)$ is J_1 and the positive contribution is J_2. In figure 5(*a*) for $k_f = 2k_1 = 100$, $J_1(k_1,k_1,2k_1) + J_2(k_1,k_1,2k_1) \approx -1.8 \times 10^{-15}$ as compared to the total flux $J(k_1) = -5.75 \times 10^{-13}$. For $k_f = 4k_1 = 200$ (figure 5*b*), $J_1(k_1,k_1,4k_1) \approx -6.59 \times 10^{-13}$, which is slightly more negative than the total value of $J(k_1)$, but $J_1(k_1,k_1,4k_1) + J_2(k_1,k_1,4k_1) \approx -3.2 \times 10^{-13}$, amounting to only 56% of the total $J(k_1)$. For $k_f = 525$ (figure 5*c*), $J_1(k_1,k_1,k_f) \approx -7.65 \times 10^{-13}$ and $J_1(k_1,k_1,k_f) + J_2(k_1,k_1,k_f) \approx -4.2 \times 10^{-13}$. Finally, for $k_f = 925$ (figure 5*d*), $J_1(k_1,k_1,k_f) \approx -9.2 \times 10^{-13}$ and $J_1(k_1,k_1,k_f) + J_2(k_1,k_1,k_f) \approx -5.75 \times 10^{-13} = J(k_1)$. One sees that there is a cancellation between J_2 and the portion of J_1 with $p, q > 4k_1$ such that the total flux is given approximately by J_1 with $p, q < 4k_1$. Thus the transfer of energy from high to low wavenumbers occurs locally, where by locally we mean through triad interactions in which the ratio of the largest leg to the smallest leg is less than about $n = 4$, while the contribution from non-local interactions is cancelled by the transfer of energy from low to high wavenumbers.

The result that $J(k_1)$ can be approximated by $J_1(k_1,k_1,4k_1)$ was verified for all inertial range wavenumbers in both the 2048^2 and the 512^2 simulations. The result also holds

FIGURE 6. Vorticity field for the 512^2 run at time t_2 of figure 3.

after formation of the condensate in the 512^2 run. The fact that the magnitude of J_1 continues to grow as k_f approaches the highest wavenumber means that ultraviolet and infrared divergences are present in the finite system, but we have seen that they are cancelled by $J_2 > 0$. The integral J_2 is a forward flux of energy which exists because the forward flux of enstrophy is small but non-zero in the finite-box inverse-cascade range.

3.4. *Physical space*

In physical space, the observed distribution of vorticity is structureless before the formation of the condensate. In the condensate state, as energy piles up in wavenumber $k = 1$, the vorticity localizes in space until it is eventually concentrated in two vortices of opposite sign. The vorticity distribution inside of each vortex is given by $\omega \approx \omega_0(t)\exp(-ar)$ with $a \approx 2\pi/50$, which is twice the characteristic scale $2\pi/k_0$ of the force in the 512^2 run. The amplitude $\omega_0(t)$ grows in time, while the root-mean-square value ω_{rms} stays essentially constant. The maximum of vorticity increased by a factor of roughly five from the time of the condensate formation to the final time of the 512^2 simulation and reached a value $\omega_{max} \approx 25\omega_{rms}$. Figure 6 shows the three-dimensional vorticity field for the latest time.

The time development of the coherent structures is shown in figure 7. Before the formation of the condensate, the vorticity field is structureless (figure 7*b*) and the velocity statistics are essentially Gaussian. As energy starts to accumulate in $k = 1$, leading to formation of large-scale motions, the vorticity picture demonstrates the creation of somewhat larger blobs of positive and negative vorticity (figure 7*d*, *f*). At this stage the deviations from Gaussian statistics of the velocity differences at some range of small scales are detected. As the Bose condensate develops and the large-scale motions become more and more energetic, the blobs disappear in favour of two small-scale vortices located at the centres of two large eddies in the velocity field (figure 7*h*, *j*, *l*). This process is accompanied by enormous but strongly localized deviations from the Gaussian statistics indicating formation of coherent structures (figure 4). The organized motion at the large scales is due to the finite extent of the box and is not a result of nonlinear dynamics. What is remarkable, however, is that it triggers the generation of small-scale coherent motions corresponding to strong nonlinearity.

Although the vortices move randomly in space, the distance L_d between their centres is approximately constant and is equal to $L_d \approx \pi$ (half of the box size). Thus Bose condensation at $k = 1$ leads to the generation of a vortical 'dipole' characterized by the two lengthscales L_d and a^{-1}. To change the separation distance L_d of the dipole, and

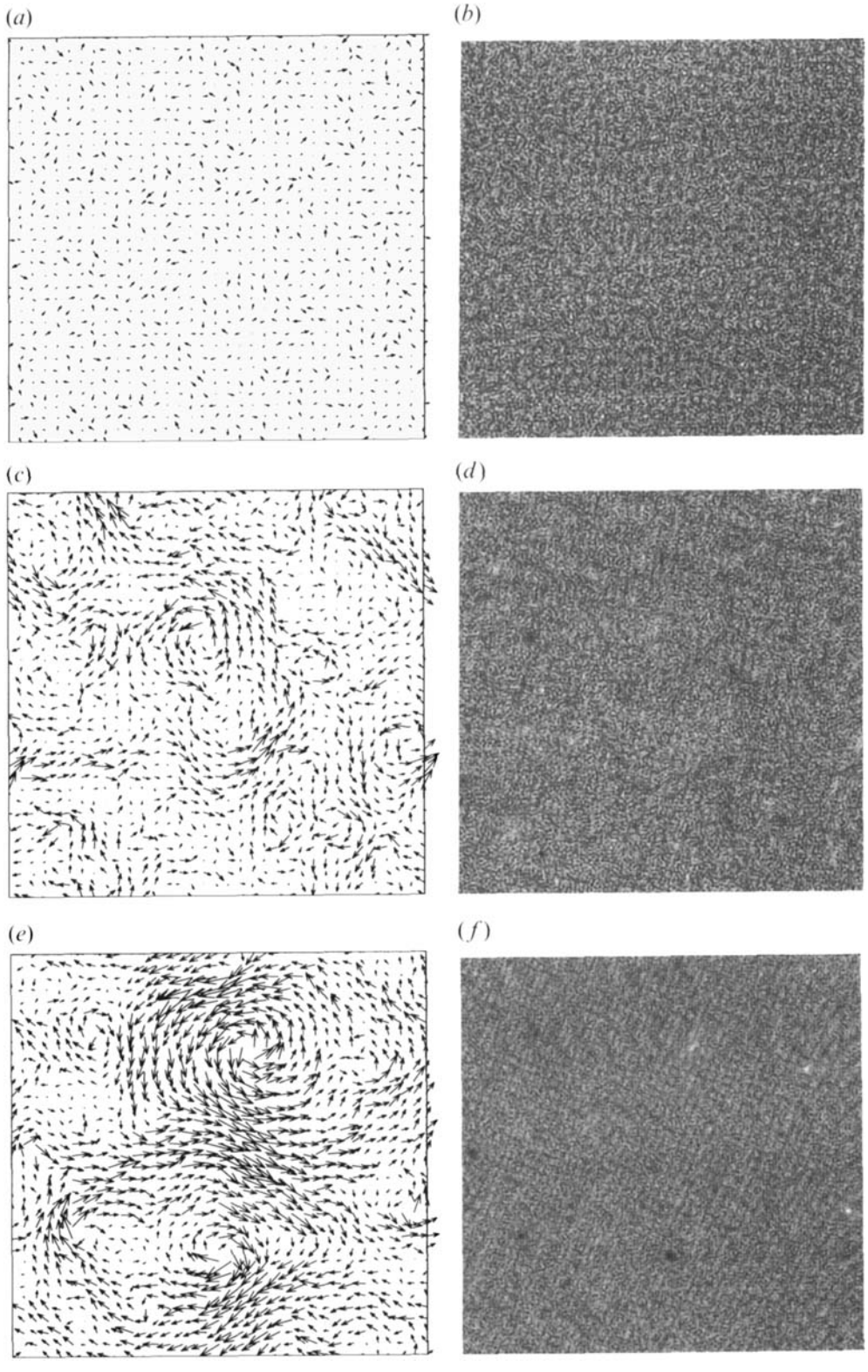

FIGURE 7(*a–f*). For caption see p. 127.

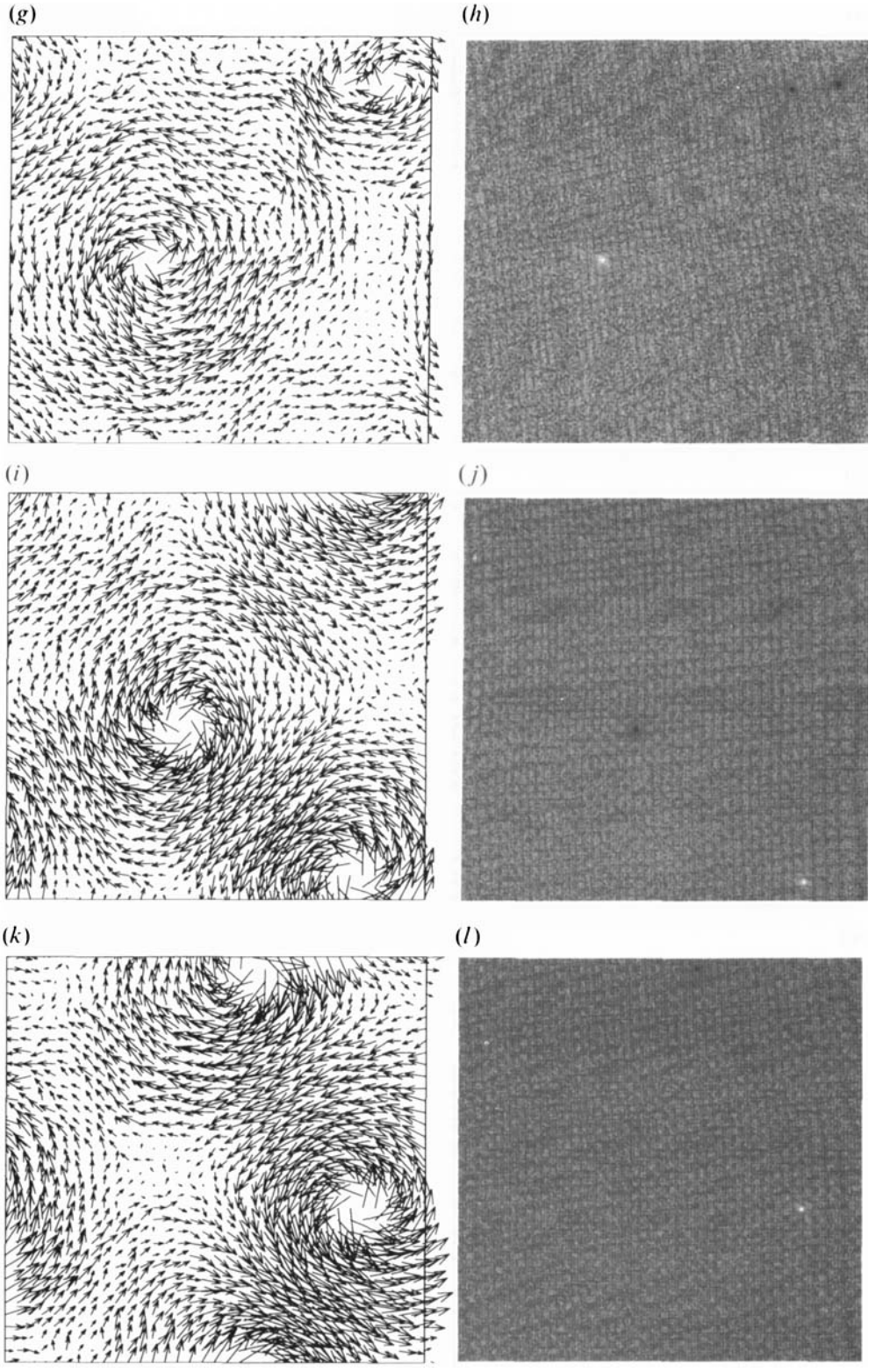

FIGURE 7(*g–l*). For caption see facing page.

to observe possible interactions between dipoles, we altered the truncation wavenumber k_T from $k_T = 1$ to $k_T = 11$. Raising the truncation wavenumber also lowers the characteristic time of evolution of the condensate and thus allows one to investigate later stages of the process. The results of the simulation with $k_T = 11$ are presented in §4.

4. Crystallization

Here we consider the case where energy is dynamically prevented from populating the largest existing scales of the system. An example of this situation is found in atmospheric turbulence, where the rotation of the earth leads to wave motions (the β-effect) that inhibit the energy cascade to scales larger than $O(10000)$ kilometres (Rhines 1975; Pedlosky 1979; Maltrud & Vallis 1991). To mimic this kind of blocking effect, we eliminated the modes $1 \leqslant k \leqslant 10$ from the box by setting the amplitudes $\boldsymbol{v}(\boldsymbol{k})$ of these modes to $\boldsymbol{v}(\boldsymbol{k}) = 0$ at each timestep. We refer to the wavenumber of the smallest non-zero mode as the truncation wavenumber k_T, and in this case $k_T = 11$. Starting again from initial condition $\boldsymbol{v}(\boldsymbol{k}) = 0$ for $0 \leqslant k \leqslant 512$, we followed the time development of the energy spectrum and velocity statistics, where the other parameters were the same as in the 512^2 run with $k_T = 1$, namely $k_0^l = 100$, $k_0^h = 105$, $A = 0.01$ and $\nu = 4 \times 10^{-36}$.

The pre-condensate development of the energy spectrum is exactly as described in §2. At first, when the nonlinearity is small compared to the forcing, the energy spectrum scales as $E(k) = a(t)\,k^0$ for $k < k_0^l$, where $a(t)$ increases as t increases. When the energy level of wavenumbers $k < k_0^l$ reaches approximately the energy level of the forced modes in $k_0^l \leqslant k \leqslant k_0^h$, the spectrum scales as $E(k) \propto k^{-5/3}$ for $k_i(t) < k < k_0^l$, where $k_i(t)$ decreases according to (8). During the time when $k_i(t) > k_T = 11$, the normalized even-order moments of velocity differences have near-Gaussian values and the vorticity field is structureless.

When the inverse integral scale $k_i(t)$ reaches $k_T = 11$, a condensate develops and like-signed vorticity begins to coagulate, eventually forming small-scale vortices. Before condensation, the coherence needed for the formation of small-scale structures is continuously destroyed by the creation of larger and larger eddies as $k_i(t)$ decreases. In the case of $k_T = 11$, the vorticity field organizes into a lattice structure of $k_T^2 = 121$ pairs of oppositely signed vortices (see figure 8). The fact that there are 121 pairs is a consequence of the imposed periodicity 11, but the regular lattice structure of the pairs themselves implies that there are longer-range correlations between the dipoles, thus the analogy with crystallization.

As the energy is increased further, it also begins to pile up at the harmonics of the cutoff $k_T = 11$, reflecting the long-range correlations and the perfection of the lattice. At these later times, the spectrum is approximated by

$$E(k) \approx \sum b_m(t)\,\delta(k - mk_T) + C_K \epsilon^{2/3} k^{-5/3}, \tag{15}$$

for $k_T \leqslant mk_T \leqslant k_0^l, m = 1, 2, 3, \ldots$ in the range $k_T \leqslant k < k_0^l$. Figure 9 displays the

FIGURE 7. Six pairs at six sequential times of the 512^2 run: (*a*), (*c*), (*e*), (*g*), (*i*) and (*k*) show velocity vectors; (*b*), (*d*), (*f*), (*h*), (*j*) and (*l*) show the vorticity field. The lowest (highest) value of vorticity is white (black). At the time of (*a*, *b*) there is negligible energy in modes with $k = O(1)$. Population of modes with $k = O(1)$ is occurring in (*c*, *d*) and (*e*,*f*). The times of (*g*, *h*), (*i*,*j*) and (*k*,*l*) are after condensation.

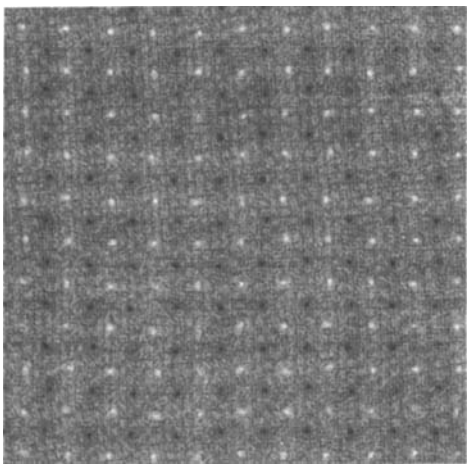

FIGURE 8. Vorticity field for the 512^2 run with $k_T = 11$ at a time well after condensation.

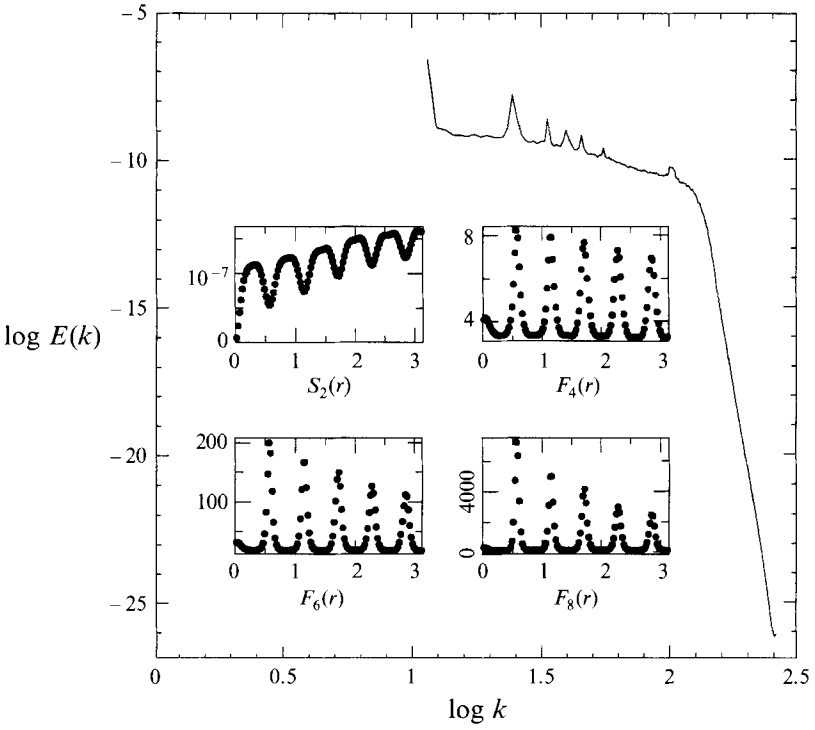

FIGURE 9. The energy spectrum for the 512^2 run with $k_T = 11$ at a time during the crystallization process. Insert: S_2 and F_{2n}, $n = 2-4$.

energy spectrum at a time when energy pile-up can be seen at wavenumbers 11, 22, 33, 44, 55 and 66. Notice that the energy spectrum remains quasi-steady with scaling exponent $x \approx \frac{5}{3}$ at wavenumbers between the harmonics. The insert of figure 9 shows the normalized even-order moments of velocity differences at the same time. The moments depart from the Gaussian values at the forcing scale, but this effect is overshadowed by the much larger departure from Gaussianity at the $k_T - 1 = 10$ scales

$2\pi m/k_T$, $m = 1, k_T - 1$. These are all the scales at which coherence is established owing to the elimination of wavenumbers $1 \leqslant k \leqslant 10$. At even later times, it is expected that the form of the spectrum (15) will break down, leading to an exponent $x > \frac{5}{3}$.

5. Application to the atmospheric spectrum

In this section we consider the effect of linear damping at the large scales corresponding to $\alpha \neq 0$. Our results suggest a possible explanation for the observed spectrum of kinetic energy in the atmosphere at wavelengths in the range 10–3000 km. We will show that the experimental data can be quantitatively explained on the basis of the theory of two-dimensional turbulence when the finite size of the system is taken into account.

5.1. *The atmospheric spectrum*

In the 1970s, wind velocity measurements were collected in a series of jet airplane trips, for example, during flights between Chicago, Los Angeles and Honolulu (Lilly & Peterson 1983; Nastrom, Gage & Jasperson 1984). Owing to the high speed of the commercial airplanes used in the experiments (≈ 1000 km h^{-1}), Taylor's hypothesis is a good approximation and can be applied to calculate the corresponding spectrum of kinetic energy for scales l in the range $l \approx$ 10–3000 km. A best fit to simple power-law behaviour $E_1(k_1) \propto k_1^{-x}$ shows that $x = \frac{5}{3}$ for wavelengths 10–300 km and $x = 2.2$–3.0 for wavelengths 1000–3000 km, where $E_1(k_1)$ is the one-dimensional spectrum of kinetic energy as a function of the wavenumber $k_1 \equiv 2\pi/l$. In addition, global data gathered at the National Meteorological Center (NMC) has been analysed to obtain the spectrum of the largest scales, indicating the scaling exponent $x \approx 3$ for l in the range 1000–3000 km (Chen & Wiin-Nielsen 1978; Boer & Shepherd 1983).

The two-dimensional Euler equations conserve both energy and enstrophy, which is the main reason why the dynamics of two-dimensional and three-dimensional flows are so different. It has not been demonstrated theoretically or numerically that a three-dimensional system of horizontal and vertical dimensions L and H, respectively, becomes two-dimensional when $H/L \to 0$. However, atmospheric motions at horizontal scales greater than $O(10)$ km are usually assumed to be quasi-two-dimensional because their vertical variation is typically of much smaller extent. Quasi-two-dimensionality is supported by the fact that stable density stratification inhibits vertical motions and tends to produce horizontal flow at large scales ($l > O(1000)$ km) (Pedlosky 1979). Thus the inertial ranges of isotropic two-dimensional turbulence (Kraichnan 1967) have played a central role in theoretical and numerical predictions of atmospheric flow. A plausible explanation for the spectrum $E_1(k_1) \propto k_1^{-5/3}$ in the range $10 < l < 300$ km is that it reflects a two-dimensional inertial energy cascade from small to large scales. According to theory, the spectrum is given by

$$E_1(k_1) = C_1 \epsilon^{2/3} k_1^{-5/3}, \tag{16}$$

where ϵ is the rate of production of kinetic energy. As shown in §3, our simulations give (9) for the two-dimensional spectrum with $\gamma \approx 0$ and with the value $C_K \approx 7.0$, which is close to the value $C_K \approx 5.8$ derived by Kraichnan (1971). Since $C_1 \approx \frac{1}{2} C_K$ in two dimensions, we use the value $C_1 = 3$ to obtain the experimental value $\epsilon \approx 10^{-5}$ m^2 s^{-1} from the airplane data.

There is substantial experimental evidence that cumulus convection clouds provide the source of energy for the larger mesoscales (Kornegay & Vincent 1976; Vincent & Schlatter 1979). Vincent & Schlatter (1979) gave an estimate for the rate of kinetic energy generation $W \approx 1$ W m^{-2} in the layer corresponding to the pressure variation

$200 < p < 700$ mb. Taking the median density of air $\rho \approx 0.5$ kg m^{-3} and the depth of the layer $h \approx 10000$ m gives $\epsilon_{cc} = W/(h\rho) \approx 2 \times 10^{-4}$ m^2 s^{-3}. It was also found that a substantial portion of the energy generated in the cumulus clouds is transported to the synoptic scales. After comparison with the estimate of ϵ obtained from the observed energy spectra we conclude that this portion is of the order 5%.

According to the theory of two-dimensional turbulence with a source of enstrophy at lengthscales $l = O(l_0)$, the spectrum $E(k) \propto k^{-5/3}$ is generated at $l > l_0$, while the spectrum $E(k) \propto k^{-3}$ is expected at $l < l_0$. This contradicts the atmospheric data, which shows an approximate -3 scaling at scales much larger than the scales corresponding to cumulus convection.

Nevertheless, the shape of the energy spectrum in the range $1000 < l < 3000$ km led investigators to suppose that the scaling $E_1(k_1) \propto k_1^{-3}$ reflects a two-dimensional inertial enstrophy cascade (e.g. Leith 1971; Lilly 1972). If this is so, then a source of enstrophy must then exist at even larger scales, and has usually been identified with the baroclinic instability (Pedlosky 1979). However, the baroclinic instability depends on the existence of a vertical shear and thus its description requires a quasi-two-dimensional (rather than strictly two-dimensional) model of atmospheric flow. Salmon (1978, 1980) studied the baroclinic instability in the context of the quasi-two-dimensional quasi-geostrophic equations formulated by Charney (1971). His numerical calculations address the data at scales 1000–3000 km, but not the statistics of smaller scales.

The existence of an energy source at large scales seemed to confuse the issue of whether the $k^{-5/3}$ spectrum for $10 < l < 300$ km is two- or three-dimensional in nature. However, closure calculations (Lilly 1989) and direct simulations (Maltrud & Vallis 1991) of two-dimensional turbulence with forcing at both high and low wavenumbers have demonstrated that an inverse cascade (towards smaller wavenumbers) of energy can coexist almost independently with a forward cascade (towards larger wavenumbers) of enstrophy. Thus a quasi-two-dimensional description remains a possibility for the entire range of scales resolved by the airplane measurements.

The view adopted here is that the spectrum of kinetic energy in the atmosphere for scales $10 < l < 3000$ km can be quantitatively described by a model based on two-dimensional turbulence. If this is so, then there is an additional mechanism leading to the k^{-3} scaling at large scales that has previously been overlooked. As mentioned in §4, the earth's rotation leads to increasingly zonal flow with decreasing wavenumber, whereby the nonlinear transfer of energy to lower wavenumbers is inhibited by the excitation of waves (the β-effect). The β-effect of the earth's rotation blocks the energy cascade to scales larger than $O(10000)$ km. Thus, given an energy source at small scales $k = O(10)$ km, there may be a pile-up of energy at scales smaller than $O(10000)$ km. When this growth is balanced by Ekman friction, a statistically steady state can be achieved with two scaling regimes: the spectrum is given by $E(k) \propto k^{-5/3}$ for $O(10) < l < 2\pi/k_\alpha$ km and $E(k) \propto k^{-3}$ for $2\pi/k_\alpha < l \ll O(10000)$ km. As will be shown below, an estimate of the Ekman damping frequency shows that this balance predicts a crossover wavenumber k_α in agreement with the airplane data.†

5.2. *The numerical simulation*

Here we present the steady-state solution to (1) with $p = 8$, $\nu = 4.0 \times 10^{-36}$ and $\alpha = 2.0 \times 10^{-6}$ at a resolution of 512^2 Fourier modes. The force f is again given by (2), where $D(k) = A^2 k^{-6}/\Delta t$ in the range $k_0^l \leqslant k \leqslant k_0^h$ with $k_0^l = 100$, $k_0^h = 105$ and $A = 0.01$.

† It has recently been shown that simulations of β-plane turbulence lead to an improved model of the atmospheric spectrum where the pile-up of energy occurs at a large scale which is smaller than the system size and determined by the value of β. This will be the subject of a future publication.

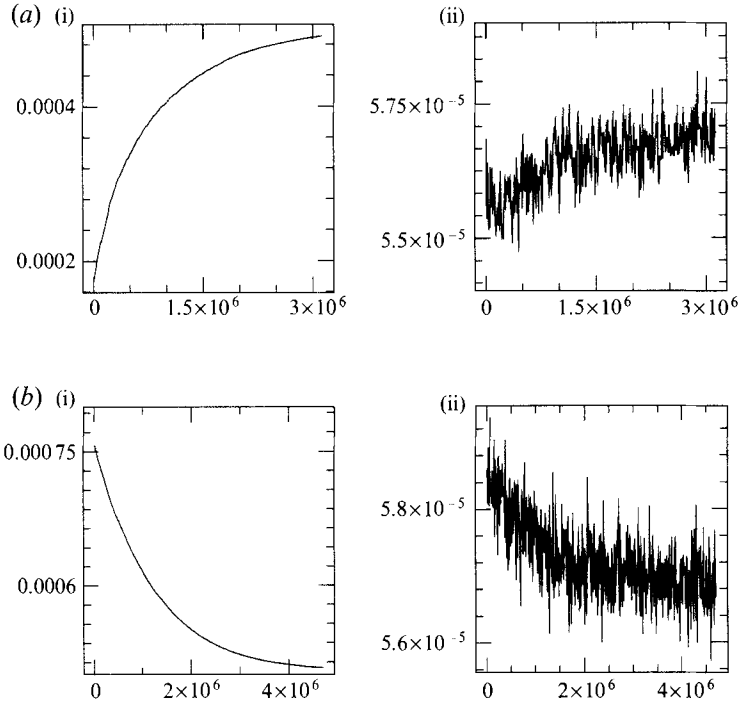

FIGURE 10. (i) v_{rms}; (ii) ω_{rms} *vs.* the number of iterations: (*a*) run_1^x; (*b*) run_2^x.

To check that the final state does not depend on initial conditions, we started both from a zero initial field with $E(k) = 0$ for all k (run_1^x), and from the long-time results of a simulation with $\alpha = 0$ and all other parameters as above (run_2^x). As can be seen from the evolution of v_{rms} and ω_{rms} in the two runs (figure 10), the same steady state was approached in both cases. Figure 11(*a*) shows the energy spectrum of run_2^x averaged over the last 6×10^5 timesteps. Even though this is a relatively short-time average, one sees that there are two distinct regimes such that the spectrum is given by

$$E(k) \approx C_\alpha k^{-y} H(k_\alpha - k) + C_K \epsilon^{2/3} k^{-5/3} H(k - k_\alpha), \tag{17}$$

where C_α is dimensional, $C_K \approx 7.0$, $H(x) = 0$ for $x \leqslant 0$ and $H(x) = 1$ for $x > 0$. Figures 11(*b*, *c*) show the averaged spectrum compensated by $k^{-5/3}$ and $k^{-2.5}$, respectively. The crossover wavenumber k_α dividing the two scaling laws should be such that the timescale of the frictional force α^{-1} and the Kolmogorov timescale $(\sigma \epsilon^{1/3} k^{2/3})^{-1}$ are equal. Kraichnan (1971) estimated that $\sigma = O(10^{-1})$ leading to $k_\alpha \approx 0.06$ in our simulation, indicating that the wavenumber region $1 \leqslant k < 5$ with spectrum $E(k) \propto k^{-y}$, $y \approx 2.5$ is an overlap region between the two scaling regimes with spectra $E(k) \propto k^{-3}$ for $k < k_\alpha$ and $E(k) \propto k^{-5/3}$ for $k > k_\alpha$. Figure 11(*d*) shows the time-averaged energy flux $J(k)$ of the same run. For wavenumbers $5 < k < k_0^l$, the flux is the constant value $J(k) \approx -2 \times 10^{-12}$. The constant flux and energy spectrum $E(k) \propto k^{-5/3}$ for $5 < k < k_0^l$ indicate that the effect of the Ekman friction is negligible for wavenumbers in this range. For wavenumbers smaller than $k \approx 5$, the flux varies smoothly from $J(5) \approx -2 \times 10^{-12}$ to $J(0) = 0$.

The steady-state vorticity field has the same dipole structure characteristic of the condensate (figure 12). The damping coefficient α determines the maximum value of the energy $E(1)$ and the maximum amplitude ω_0 of the vorticity. The amplitude ω_0 in our

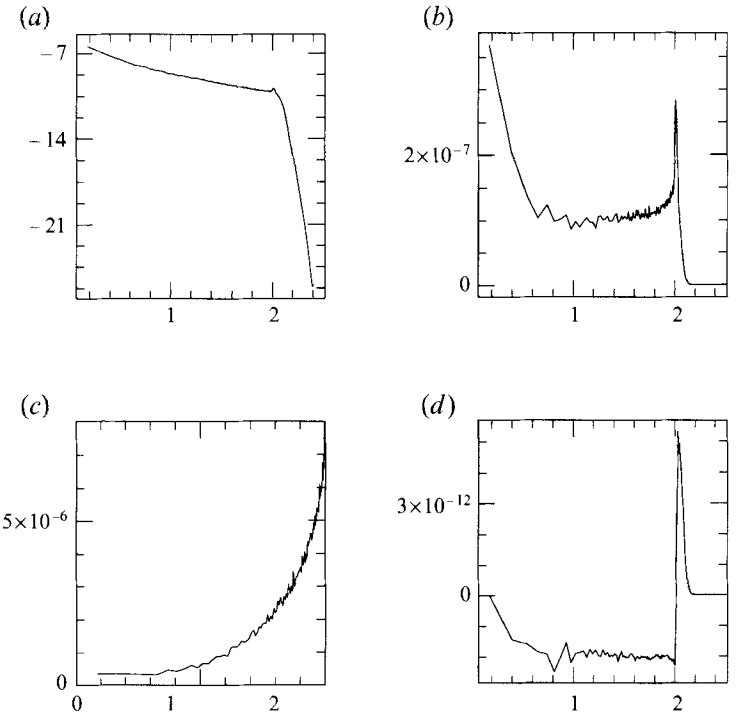

FIGURE 11. For run$_2^x$ averaged over the last 6×10^5 timesteps (*a*) $E(k)$; (*b*) $k^{5/3}E(k)$; (*c*) $E^{2.5}E(k)$; (*d*) $J(k)$.

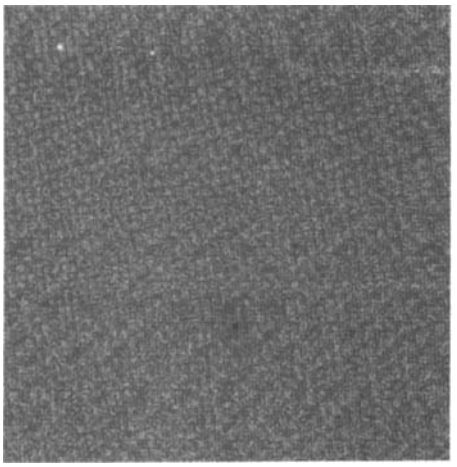

FIGURE 12. Steady-state vorticity field of run$_2^x$.

simulation is approximately 15 times larger than the root-mean-square value ω_{rms}. In the case of the atmosphere, the β-effect arrests the energy cascade at a scale much smaller than the circumference of the earth, and thus we expect the vorticity field to be characterized by many coherent vortices similar to the simulation with $k_T = 11$ discussed in §4. A preliminary study shows that the number of coherent vortices increases with increasing rotation rate.

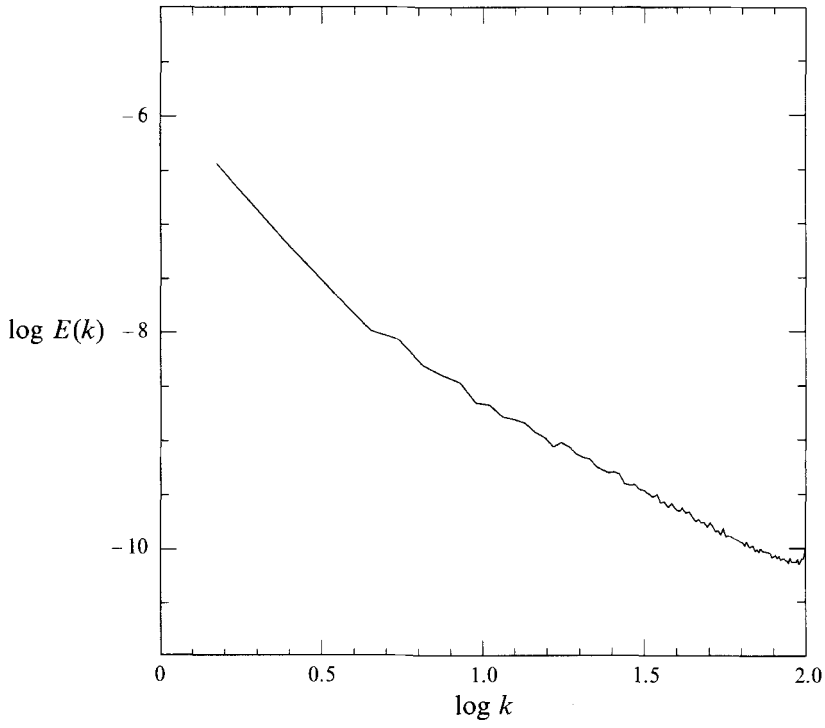

FIGURE 13. Close-up of figure 11(*a*) for $1 \leqslant k \leqslant k_0^l = 100$.

Figure 13 is a close-up of the spectrum at scales larger than the forcing scale to emphasize its similarity to the atmospheric spectra measured by aircraft. Lilly & Peterson (1983) report $x \approx \frac{5}{3}$ for wavelengths of less than about 150 km and $y \approx 2.2$ at larger scales. Nastrom, Gage & Jasperson (1984) estimate $x \approx \frac{5}{3}$ for wavelengths in the range 2.6–300 km and $y \approx 3$ in the range 1000–3000 km. The frequency α is approximately $\alpha \approx 1/10$ days^{-1} corresponding to $\alpha \approx 10^{-6}$ s^{-1}, and the value of the dissipation rate from the data is $\epsilon = O(10^{-5})$ m^2 s^{-3}. These experimental parameters and Kraichnan's (1971) estimates of $\sigma = O(10^{-1})$ give for the experimental crossover wavenumber $k_\alpha = O(10^{-5})$ m^{-1}, which is in agreement with the observations. Notice that it is impossible for damping at the smallest wavenumbers $k < k_\alpha$ to cause a direct transition from the Kolmogorov spectrum $E(k) \propto k^{-5/3}$ at $k > k_\alpha$ to a steeper spectrum at $k < k_\alpha$ unless there is a competing mechanism for growth of energy in $k < k_\alpha$, in this case the formation of a condensate due to the finite extent of the domain. Since the atmosphere above the earth is essentially within a periodic 'box', our simulations suggest that the steeper spectrum observed for the large scales $1000 < l < 3000$ km might originate from the finite size of the earth and the Ekman boundary layer.

We have shown that the atmospheric spectrum of kinetic energy in the entire range 10–3000 km is given with quantitative agreement by the theory of forced two-dimensional turbulence when finite-size effects are taken into consideration. A statistically steady state is achieved by the balance between Bose condensation and Ekman damping. Although two-dimensional turbulence without rotational effects is a crude approximation to geostrophic flows, Bose condensation remains a possibility owing to the finite size of the atmosphere. In this case, the system is unstable to formation of small-scale violent supervortices. Thus, the large and small-scale dynamics are strongly coupled. The role of this coupling in the atmosphere is still

unclear and deserves a detailed investigation. Ongoing work includes the further numerical study of two-dimensional turbulence on a rotating sphere. Future calculations should attempt to determine the relative importance of the baroclinic instability and Bose condensation in the generation of the k^{-3} spectrum. The NMC global data set shows that there is a forward flux of energy in some range of large scales (see e.g. Boer & Shepherd 1983).

In order to experimentally verify the physical mechanisms described in this section, accurate experimental data on the energy flux as a function of wavenumber are necessary. It should be emphasized that, at the synoptic scales where the wind speed reaches 300 km h^{-1}, Taylor's hypothesis cannot be used unless high-speed aircraft are employed.

6. The mechanism of structure generation

To understand the mechanism of the small-scale structure generation described in the previous sections, let us recall the vorticity-generation process in the enstrophy range with spectrum $E(k) \propto k^{-x}$ for $x > 3$. In this case, vorticity is produced at the forcing scale in the form of blobs which are sheared by the energetic large-scale motions in the fluid. This process leads to thinning of the blobs and, as a consequence, vorticity is transferred to small scales where it is eventually dissipated by the viscous mechanism (Kraichnan 1974; Kraichnan & Montgomery 1980). In the system considered in this work, the shear in the flow characterized by the $k^{-5/3}$ energy spectrum is not strong enough to generate small-scale structures. This period of flow evolution is dominated by the inverse energy cascade: creation of large-scale motions as a result of the nonlinear interaction between smaller-scale velocity fluctuations. This process does not generate large-scale enstrophy. The situation changes with the initiation of box-size motions and the steepening of the energy spectrum. Then the large-scale shear in the system is no longer small and enstrophy is generated at $k = 1$. Vorticity blobs are formed at the large scales and then destroyed in the strong-shear regions of the flow owing to shear-induced thinning. However, vorticity is accumulated at the centres of the large-scale motions predominantly characterized by closed streamlines.

This process is similar to the one considered by Kraichnan (1970) in his numerical experiments of turbulent diffusion. In three-dimensional flow, the process was well approximated by an effective diffusivity. However, in two dimensions, the effective-diffusivity approximation failed. There, the high probability of 'trapping trajectories' led to particle accumulation in some localized regions of the flow. In the system considered in this work the trapping trajectories of vorticity, convected by the velocity field, are much more prominent because of finite-size effects forcing circular fluid streamlines. This picture of vortex formation is illustrated in figure 7 presenting the time sequence of both velocity and vorticity fields starting from the structureless state. Before population of the modes with $k = O(1)$ (figure 7*a*, *b*), the velocity field seems entirely random and the vorticity field, in turn, does not show any organization. Later, when $k_i \approx 1$ one notices some large-scale structure in the velocity field, accompanied by creation of rather diffuse and shapeless vorticity blobs situated within closed streamlines (figure 7*c–f*). As the amplitude of the condensate grows and the velocity is organized into a powerful flow with characteristic length approximately equal to the half-box size (figure 7*g–l*), the vorticity blobs are thinned and destroyed by the strong shear, and can survive only in the vicinity of the centres dominated by the closed streamlines ('safe havens' according to J. McWilliams).

The later stages of the evolution, described in §4, can be understood in the following

way. When time $t \to \infty$, the enstrophy Ω in the system cannot be considered constant since

$$\Omega(t) \approx b(t) k_T^2 + \Omega_s, \tag{18}$$

where Ω_s is the contribution to the total enstrophy from the scales $k > k_T$. Ω_s dominates the enstrophy at times $t < t_s$, where t_s is found from the relation $b(t_s) k_T^2 = \Omega_s$. We remind the reader that k_T is the smallest infrared wavenumber. Thus, in a finite system the inverse energy cascade and Bose condensation serve as an effective infrared source of vorticity. The strong large-scale shear, present at late stages of evolution, produces the thinning effect discussed above and, as a consequence, enstrophy is transferred to smaller scales in a manner similar to that in Kraichnan's (1974) classic picture of the direct enstrophy cascade. This process competes with the inverse-enstrophy cascade owing to the development of the condensate. Since the enstrophy flux in a statistically steady state must be constant, zero or otherwise, it may well be that a non-equilibrium steady state in this system is impossible. This is suggested by the growing-in-time peaks in the energy spectrum shown in figure 9. What we have just described is a novel mechanism: the nonlinear term in the equation of motion serves as an infrared source of vorticity and, in addition, transfers newly created vorticity to the smaller scales. This differs from a typical situation in which enstrophy is produced by external forces and fields, and then transferred to the smaller scales by the nonlinear interaction.

7. Discussion

The first basic assumption of a typical analytical theory of turbulence is the existence of a statistically steady flow governed by the Navier–Stokes equations. In three dimensions, this usually implies a large-scale stirring mechanism and small-scale viscous dissipation. In the intermediate range of scales where both production and dissipation can be neglected, energy conservation leads to constancy of the energy flux in wavevector space, and the goal of the theory is to find solutions corresponding to this constant flux.

In two-dimensional turbulence, the situation is more complicated. Owing to the second conservation law, there exist energy and enstrophy fluxes towards large and small scales, respectively. Since viscous dissipation is negligible in the limit $k \to 0$, a steady state can be maintained only if another dissipation mechanism is assumed at the largest scales. This is an additional assumption of the theory since the Navier–Stokes equations do not have this dissipation and introduction of external fields is necessary. To illustrate how an artificial large-scale dissipation can modify the physics of two-dimensional turbulence, let us consider the expression for the enstrophy flux $J_\Omega(k)$ for $k < k_0$,

$$J_\Omega(k) = 2\nu \int_1^k z^{2+x} E(z)\, \mathrm{d}z, \tag{19}$$

where x is the power of the Laplacian in the dissipation term. In the case of the Navier–Stokes equations, $x = 2$ and the integral is asymptotically equal to zero for the energy spectrum $E(z) \propto z^{-y}$ with $y < 5$. However, in the case of an artificial dissipation where x is a large negative number, the integral (19) diverges in the small-k limit, and the enstrophy flux is finite in the range $1 < k < k_0$. This is a two-flux state for which no theory exists. The non-zero negative enstrophy flux is likely to introduce important modifications to the physics of the flow. Indeed, enstrophy is created at small scales in the form of statistically independent positive and negative vortices. The only way for

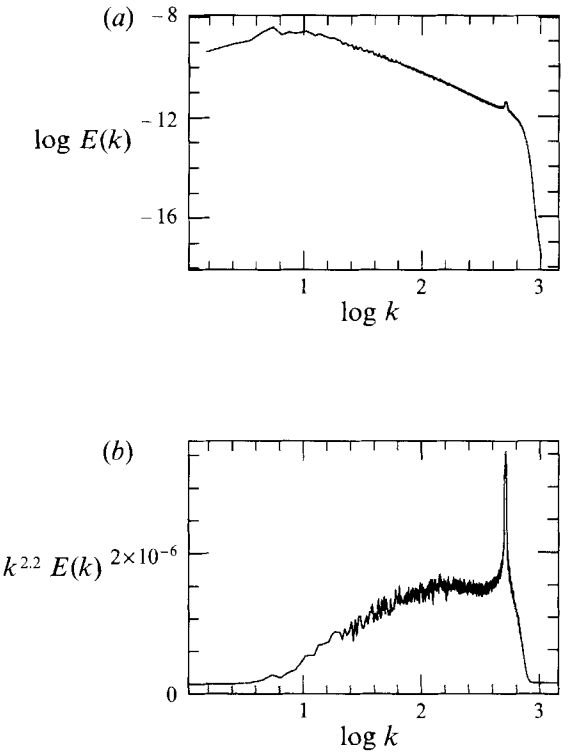

FIGURE 14. (*a*) $E(k)$ and (*b*) $k^{2.2}E(k)$ for the 2048^2 run with $\nu = 3.0 \times 10^{-48}$ to allow for a significant forward cascade of enstrophy. This is not a quasi-steady state.

enstrophy to be transferred to the large scales is through the process of same-sign vortex merger. This dynamics is very different from the inverse-cascade of energy towards the large scales that does not generate large-scale vorticity.

Demonstration of the statistically quasi-stationary state, characterized by non-trivial energy spectrum but having close-to-Gaussian statistics is one of the main results of this paper. The parameters of the problem were chosen such that no substantial direct enstrophy cascade was present. This choice minimizes the nonlinear interaction between the modes in the intervals $k > k_0$ and $k < k_0$. In this case, the small-scale dynamics are dominated by the random force acting in the vicinity of $k = k_0$ and not by the nonlinearity as in three-dimensional turbulence. The simplicity of the small-scale dynamics is partly responsible for both the close-to-Gaussian statistics of the velocity field and the Kolmogorov spectrum $E(k) \propto k^{-5/3}$. This statement has been confirmed by numerical simulations in which the magnitude of the hyperviscosity was reduced to allow formation of some enstrophy range. For the value $\nu = 3.0 \times 10^{-48}$, the exponent of the energy spectrum for $k_i(t) \ll k < k_0^l$ changed to $2 \leqslant x < 2.3$ and a quasi-stationary state was not obtained. Figures 14(*a*, *b*) show the energy spectrum $E(k)$ and compensated spectrum $k^{2.2}E(k)$, respectively, at a time when the inverse-integral scale is $k_i(t) \approx 10$. The change in the exponent was accompanied by the generation of small-scale vortices. This fact shows that energy is produced at $k \approx k_0$ and that the vortices are generated owing to the direct enstrophy cascade at $k > k_0$. These are not the vortices due to finite-size effects, and we call them the ultraviolet vortices. The ultraviolet vortices are responsible for intermittency at scales $r = O(k_0^{-1})$, but the $F_{2n}(r)$, $n = 2-4$ remain the Gaussian values for $r > 0.1$. When large-magnitude vorticity was

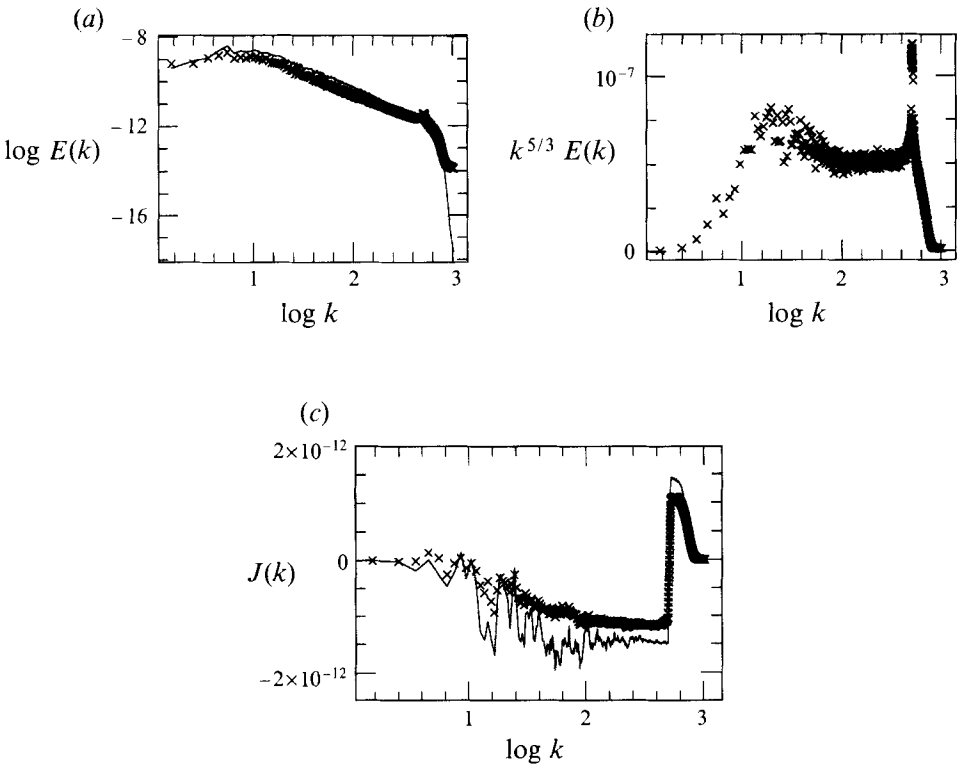

FIGURE 15. (*a*) $\log E(k)$ for the unfiltered (solid) and filtered (crosses) fields. (*b*) $k^{5/3}E(k)$ for the filtered field. (*c*) The flux $J(k)$ for the unfiltered (solid) and filtered (crosses) fields.

filtered out, the remaining structureless velocity field had the Kolmogorov spectrum. Figure 15(*a*) compares the spectra of the unfiltered (solid curve) and filtered (crosses) fields. Figure 15(*b*) is the compensated spectrum $k^{5/3}E(k)$ for the filtered field including only $|\omega| < 3\omega_{rms}$. The threshold $3\omega_{rms}$ was found to be the smallest integer multiple of ω_{rms} for which the field filtered above this threshold retained a constant flux in $k_i(t) \ll k < k_0^l$. Although only about 50% of the energy in the range $k < k_0^l$ remains in the filtered field, figure 15(*c*) shows that the background carries about 80% of the energy flux. In figure 15(*c*), the unfiltered and filtered fluxes are shown respectively by the solid curve and crosses. Thus in this range of parameters energy is mainly transferred in the $k^{-5/3}$-Kolmogorov background field.

We would like to acknowledge many helpful discussions with V. Borue, E. Jackson, R. H. Kraichnan, C. E. Leith, D. K. Lilly, J. C. McWilliams, A. Polyakov and R. Salmon. We are grateful for the support of ONR N00014-92-C-0089 and ONR/ARPA N 00014-92-J-1363.

REFERENCES

BENZI, R., PATERNELLO, S. & SANTANGELO, P. 1988 Self-similar coherent structures in two-dimensional decaying turbulence. *J. Phys.* A **21**, 1221–1237.

BOER, G. J. & SHEPHERD, T. G. 1983 Large-scale two-dimensional turbulence in the atmosphere. *J. Atmos. Sci.* **40**, 164–184.

CHARNEY, J. G. 1971 Geostrophic turbulence. *J. Atmos. Sci.* **28**, 1087.

CHEN, T.-C. & WIIN NIELSEN, A. 1978 Nonlinear cascades of atmospheric energy and enstrophy in a two-dimensional spectral index. *Tellus* **30**, 313–322.

FLIERL, G. R., STERN, M. E. & WHITEHEAD, J. A. 1983 The physical significance of modons. Laboratory experiments and general integral constraints. *Dyn. Atmos. Oceans* **7**, 233–263.

FRISCH, U. & SULEM, P. L. 1984 Numerical simulation of the inverse cascade in two-dimensional turbulence. *Phys. Fluids* **27**, 1921–1923.

HOSSAIN, M., MATTHAEUS, W. H. & MONTGOMERY, D. 1983 Long-time state of inverse cascades in the presence of a maximum length scale. *J. Plasma Phys.* **30**, 479–493.

JACKSON, P. E., SHE, Z. S. & ORSZAG, S. A. 1991 A case study in parallel computing: homogeneous turbulence on a hypercube. *J. Sci. Comput.* **6**, 27.

KOLMOGOROV, A. N. 1941 Energy dissipation in locally isotropic turbulence. *Dokl. Akad. Nauk SSSR* **32**, 19–21.

KORNEGAY, F. C. & VINCENT, D. G. 1976 Kinetic energy budget analysis during interaction of tropical storm Candy (1968) with an extratropical frontal system. *Mon. Weather Rev.* **104**, 849–859.

KRAICHNAN, R. H. 1967 Inertial ranges in two-dimensional turbulence. *Phys. Fluids* **10**, 1417–1423.

KRAICHNAN, R. H. 1970 Diffusion by a random velocity field. *Phys. Fluids* **13**, 22–31.

KRAICHNAN, R. H. 1971 Inertial-range transfer in two- and three-dimensional turbulence. *J. Fluid Mech.* **47**, 525–535.

KRAICHNAN, R. H. 1974 Convection of a passive scalar by a quasi-uniform random straining field. *J. Fluid Mech.* **64**, 737–762.

KRAICHNAN, R. H. & MONTGOMERY, D. 1980 Two-dimensional turbulence. *Rep. Prog. Phys.* **43**, 547–615.

LEITH, C. E. 1971 Atmospheric predictability and two-dimensional turbulence. *J. Atmos. Sci.* **28**, 145–161.

LILLY, D. K. 1972 Numerical simulation studies of two-dimensional turbulence: I. Models of statistically steady turbulence. *Geophys. Fluid Dyn.* **3**, 289–319.

LILLY, D. K. 1989 Two-dimensional turbulence generated by energy sources at two scales. *J. Atmos. Sci.* **46**, 2026–2030.

LILLY, D. K. & PETERSON, E. L. 1983 Aircraft measurements of atmospheric kinetic energy spectra. *Tellus* **35A**, 379–382.

MCWILLIAMS, J. C. 1989 Statistical properties of decaying geostrophic turbulence. *J. Fluid Mech.* **198**, 199–230.

MALTRUD, M. E. & VALLIS, G. K. 1991 Energy spectra and coherent structures in forced two-dimensional and beta-plane turbulence. *J. Fluid Mech.* **228**, 321–342.

MELANDER, M. V., ZABUSKY, N. J. & MCWILLIAMS, J. C. 1987 Asymmetric vortex merger in two dimensions: Which vortex is 'victorious'? *Phys. Fluids* **30**, 2610–2612.

MELANDER, M. V., ZABUSKY, N. J. & MCWILLIAMS, J. C. 1988 Symmetric vortex merger in two dimensions: causes and conditions. *J. Fluid Mech.* **195**, 303–340.

MONIN, A. S. & YAGLOM, A. M. 1975 *Statistical Fluid Mechanics*, vol. 2. MIT Press.

NASTROM, G. D., GAGE, K. S. & JASPERSON, W. H. 1984 Kinetic energy spectrum of large-scale and mesoscale atmospheric processes. (Letter) *Nature* **310**, 36–38.

OVERMAN, E. A. & ZABUSKY, N. J. 1982 Evolution and merger of isolated vortex structures. *Phys. Fluids* **25**, 1297–1305.

PEDLOSKY, J. 1979 *Geophysical Fluid Dynamics*. Springer.

RHINES, P. B. 1975 Waves and turbulence on the β-plane. *J. Fluid Mech.* **69**, 417–443.

SALMON, R. 1978 Two-layer quasi-geostrophic turbulence in a simple special case. *Geophys. Astrophys. Fluid Dyn.* **10**, 25–52.

SALMON, R. 1980 Baroclinic instability and geostrophic turbulence. *Geophys. Astrophys. Fluid Dyn.* **15**, 167–211.

SMITH, L. M. & YAKHOT, V. 1993 Bose condensation and small-scale structure generation in a random force driven 2D turbulence. *Phys. Rev. Lett.* **71**, 352–355.

VINCENT, D. G. & SCHLATTER, T. W. 1979 Evidence of deep convection as a source of synoptic-scale kinetic energy. *Tellus* **31**, 493–504.